Mitigation of the Commutation Failure Problem in the HVDC Multi-Infeed Scenario in Brazil Using Synchronized Phasor Measurement

Rafael O. Fernandes
DSCE – Department of Energy Control and Systems
UNICAMP
Campinas, Brazil
r096443@dac.unicamp.br

Maria C.D. Tavares
DSCE - Department of Energy Control and Systems
UNICAMP
Campinas, Brazil
ctavares@unicamp.br

***Abstract*—This paper presents the Commutation Failure (CF) problem in the HVDC-LCC (High Voltage Direct Current - Line-Commutated Converter) scenario in Brazil through the monitoring of Short-Circuit Ratio (SCR), CF indexes, Direct Current (DC) link power, and the use of simulated synchrophasor data. The analysis was performed by training a neural network using data from the year 2020, and its robustness was verified using data from the year 2021 of the Brazilian Interconnected Power System (BIPS). Additionally, an analysis of transient instability in the North-South Transmission Corridor (NSC) will be presented right after the occurrence of CF by monitoring the Lyapunov transient instability margin, with the primary objective of bringing subsidies to the control center operation area, according to the severity of the CF occurrence, avoiding the propagation of CF, mitigating it through real-time predictive actions, such as power redispatch on DC links and, thus, minimizing the occurrence of CF.**

***Index Terms*—Commutation Failure, HVDC, Artificial Neural Network, Synchrophasor Measurement, Predictive Index.**

I. INTRODUCTION

In electrical systems with a single HVDC-LCC link for the transmission of large blocks of power over long distances, in a single infeed configuration, adopted, for example, the evaluation of an index called Effective Short-Circuit Ratio (ESCR) for alternating current (AC) substations [1]. However, currently, in Brazil and other countries of continental electrical dimensions, such as China, a DC Multi-Infeed scenario can occur, where multiple injections of large power blocks are provided by DC links that are electrically close, which means operating with multiple inverter stations connected to nearby AC busbars. The BIPS electrical operation has six HVDC bipoles installed at four inverter stations in the same Southeast geoelectric area, totaling about 20 GW of power injection, specifically 2 Madeira's bipoles interconnecting Porto Velho in the North region to Araraquara in the Southeast region, 2 Belo Monte's bipoles interconnecting Xingu in the North area to Estreito in the Southeast area and Xingu to Terminal Rio in the Southeast area and, finally, 2 Itaipu's bipoles interconnecting Foz do Iguaçu in the South area to Ibiúna in the Southeast area. A local CF can occur due to an electrical fault in the AC system, starting a few milliseconds after the occurrence of the fault. On the other hand, Simultaneous Commutation Failure (SCF) occurs when there is CF in several HVDC links, also due to a first fault in the AC network. This paper proposes using a neural network for CF pattern classification and identification and, as a complementary analysis, presents the stability margin results through Lyapunov Transient Energy Function (LTEF) on the NSC right after the CF onset. The neural network used data from different load flow and electromechanical stability simulation scenarios for the training and operation stages, considering heavy, medium, and light loads, during the years 2020 and 2021, as well as for the FET analyses. The more extensive database allowed us to obtain more robust results, even with the evolution of the electrical network.

II. COMMUTATION FAILURE PHENOMENON

The CF can occur due to poor operation during the commutation process of the thyristor valves in the converter, and most often, these result from more severe distortions or sinking of the reference voltage signals for the firing valve control, inherent to the occurrence of faults in the AC system [2-7]. In general, recovery of the HVDC link after a CF will occur with the inverter operating with an extinction angle above the minimum value adopted ($\gamma > \gamma\_min$) as the control actions momentarily advance the trigger angle α. In practice, this is reflected in an increase in the reactive power absorbed by the converter stations, lasting a few cycles until the AC voltage recovers, where the speed of recovery is given as a function of the behavior of the AC grid. During a grid fault, the fault clearing time is paramount for the adequate work of the PLL (Phase Locked Loop). However, the restoring voltage must have a sinusoidal waveform. When the CF occurs, its detector control, which compares whether the current of the valves is greater than the DC, will limit the firing angle α of the valves to give rise to the extinction angle γ.

Submitted to the 23rd Power Systems Computation Conference (PSCC 2024).

Figure 1 shows the electromagnetic transient simulation using the PSCAD tool. The database refers to Brazil's planning study model, including the six HVDC-LCC bipoles. A 100-ms single-line ground fault was simulated on the LT 500 kV Araraquara-Taubaté, observing a CF on the HVDC-LCC Madeira (Light Load Scenario, January 2021). The thyristor control system uses the three-phase voltage of the converter's primary side transformer as the reference voltage. By the valve-side currents in the secondary transformer, YY can be seen in Figure 1.

VLWY = voltage at the primary (line winding) converter transformer's inverter side.

IVWSAY, IVWSBY, and IVWSCY = valve winding currents, transformer YY, inverter side P3.

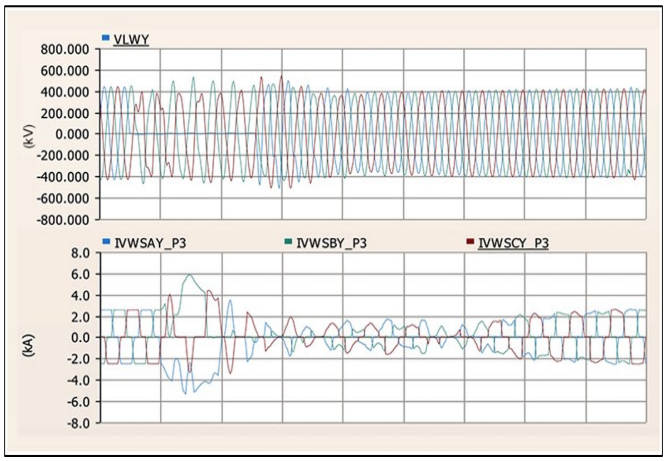

Fig 1. Commutation Failure – Madeira HVDC-LCC. Source [Authors]

A. Commutation Failure Indexes

For the CF multi-infeed problem, predictive indexes are calculated to select critical cases related to dynamic stability. Cigre [8] initially developed the calculation methodology, which is currently adopted by CEPEL [1]. Four CF indexes were used in this work, as described below.

✓ SCR (*Short Circuit Ratio*) is calculated as being:

$$SCR_i = \frac{Scc_i}{Pdc_i} \quad (1)$$

Where: S_{cci} is the three-phase short-circuit power at the inverter busbar of converter i, and P_{dci} is the power injected by converter i.

✓ MIIF (*Multi-infeed Interaction Factor*) is determined to be a relationship between the voltage variations at the busbars of interest:

$$MIIF_{j,i} = \frac{\Delta V_j}{\Delta V_i} \quad (2)$$

Where ΔV represents the voltage variation at busbars i and j, respectively.

✓ PI (*Potential of Interaction*) is calculated as a ratio of the power injected by the converters multiplied by the MIIF index.

$$PI = MIIF_{j,i}\frac{Pdc_j}{Pdc_i} \quad (3)$$

✓ MISCR (*Multi-infeed Interaction SCR*) is calculated as:

$$MISCR_i = \frac{Scc_i}{Pdc_i + \sum_j \left(MIIF_{j,i} \cdot Pdc_j\right)} \quad (4)$$

In [1], a proposal for online monitoring of the MISCR index is presented as a predictive way to provide support in decision-making to the control center operators in real-time when situations occur in which the AC hybrid network interacts with the multiple infeed HVDC-LCC systems.

III. SYNCHROPHASOR MEASUREMENT SYSTEM

A synchrophasor measurement system consists of PMU equipment installed at Transmission Line (TL) terminals or the busbars of the power grid, data concentrators, time synchronization, data storage, and real-time and offline applications. Through a data communication system, via an adequate telecommunication channel infrastructure that guarantees the minimum latency adopted in the project design, the synchrophasor quantities of voltage, current, frequency, and rate of change of frequency are sent at transmission rates, e.g., 60 fps (samples per second), via the IEEE C37.118 protocol [9],[10]. The PDC (Phasor Data Concentrator) performs the alignment and storage of the synchrophasor data and runs the applications in real-time or offline scenarios. The synchrophasor measurements need to be synchronized and present a proper time quality (timestamp) as stipulated in the IEEE standard, keeping the Total Vector Error (TVE), Frequency Error (FE), and Rate of Frequency Error (RFE) within acceptable error ranges. Due to the difficulty of obtaining synchrophasor measurements by the Transmission System Operator (TSO) involved with the analysis, the electrical quantities were simulated via the tool Anatem from CEPEL [11].

IV. ARTIFICIAL NEURAL NETWORKS

Artificial Neural Networks (ANN) can be interpreted as computational models inspired by the human nervous system [12]. They can acquire and maintain knowledge based on previous information. They are characterized by a set of artificial neurons interconnected by many interconnections (artificial synapses), represented by vectors and matrices of synaptic weights. In this paper, ANN was used, focusing on pattern recognition, and the network chosen was the Radial Basis Function (RBF). The RBF network extracts the features in the first neural layer and prepares them for use in the output layer. It uses fewer neurons than the Multilayer Perceptron (MLP) in the case of clustered samples. The second stage, associated with the adjustments of the output layer neuron weights, uses a learning criterion like that used by the MLP, the generalized delta rule.

Finally, unlike the MLP nets, the training process starts with the intermediate layer neurons and ends with the output layer neurons. Figure 2 illustrates an MLP network, and Figure 3 illustrates an RBF network.

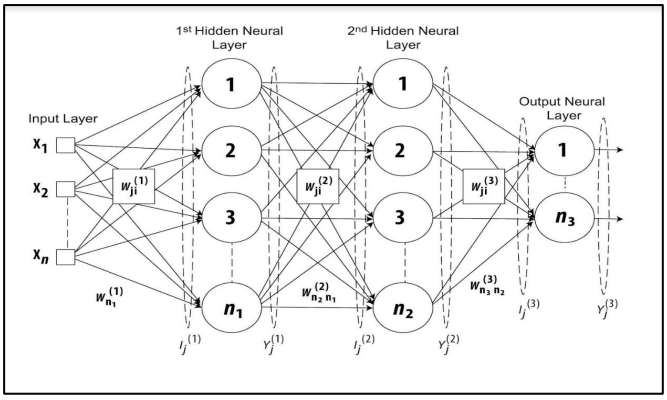

Fig. 2 – MLP Net. Source [12]

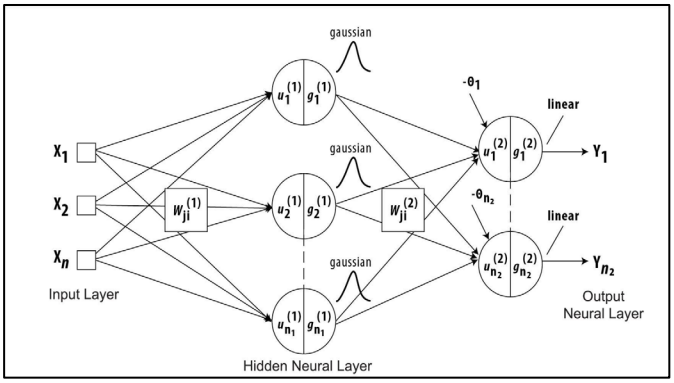

Fig. 3 – RBF Net. Source [12]

V. LYAPUNOV ENERGY FUNCTION

According to [13],[14] the second Lyapunov method allows the study of the global stability of a system under analysis to be performed directly, without the explicit solution of its nonlinear differential equations, via computer simulations in the time domain. This method attempts to determine global stability directly by using a Lyapunov function defined in a state space analysis.

A. Transient Lyapunov Energy Function

Considering a real power electrical system, constructing the Lyapunov Energy Function (LEF) is possible by assuming some simplifications, such as disregarding the transfer conductances in the network equations. In this way, obtaining the LTEF instead of the LEF is possible; with this, the Potential Energy (PE) and Kinetic Energy (KE) can be numerically obtained. The LTEF does not directly satisfy the Lyapunov conditions because part of the PE is numerically computed along the trajectory of the system, and, by definition, it is necessary to have the post-fault equilibrium angle operation for computing the PE [15]-[17].

B. Power Transferred in a Transmission Corridor

In Figure 4, there is the representation of the power transfer between two geoelectric areas, represented by the busbars of Colinas and Serra da Mesa located in the north and northeast regions in Brazil, symbolizing a transmission corridor interconnected by an equivalent reactance, which can be given by x_{eq}. The NSC presents a strong correlation between active power and angular difference It is worth noting that there is a reinforcement planned for the entry into operation of two TL between Miracema and Serra Pelada substations, and two TL between Serra Pelada and Xingu substations, as well as the entry of one more TL between Serra Pelada and Itacaiúnas substations, therefore, the correlation between active power and the angular difference in the CNS should be analyzed again after the entry into operation of these systems reinforcements.

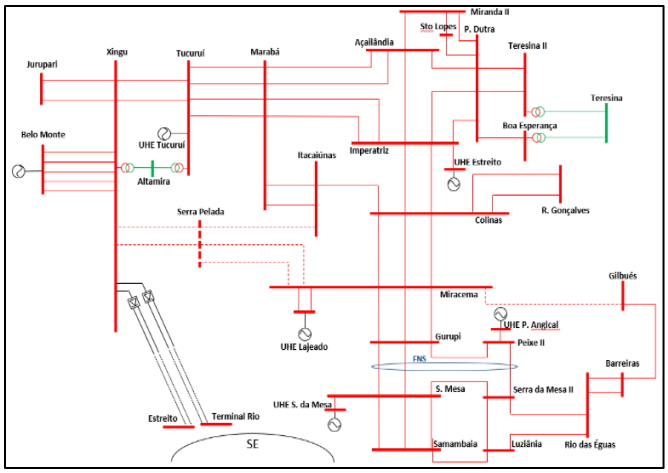

Fig. 4 – Geoelectric Area North-South/Southeast

C. LTEF Mathematical Formulation

According to [11] and [12], the PE and KE can be obtained as:

$$V_{PE} = \frac{E_1 E_2}{x'_e}(\cos(\delta_0) - \cos(\delta) + sen(\delta_{op})x(\delta_{op} - \delta)) \quad (5)$$

$$V_{KE} = \frac{1}{2}(2H)\Omega w^2 = H\Omega w^2 \quad (6)$$

Where $\delta = \delta_1 - \delta_2$, δ_1, and δ_2 are the internal angles of the generators, δ_0 is the initial fault angle, δ_{0p} is the pos-fault angle $E_1$and E_2 are the internal voltages of the generators, in p.u., $\Omega = 2\pi f$, where f is the nominal frequency of the system, in hertz, and $w = w_1 - w_2$ (angular velocities of generators 1 and 2) in p.u. The equivalent inertia, on the other hand, is given in p.u., by $H = H_1 x H_2/(H_1 + H_2)$, and the equivalent reactance x'_e, given in p.u., also includes the reactance of the transformers and the transient impedance of the generators. In possession of the phasor measurements of the busbars and circuits, one can approximate: $V_1 \approx E_1$, $V_2 \approx E_2$, $\theta \approx \delta$, $w_b \approx w$ e $x'_e \approx x_e$, where $w_b = w_{b1} - w_{b2}$, where: w_{b1} and

w_{b2} are the angular frequencies, in rad/s, respectively. The voltages on the busbars/circuits are not constant and vary with time, containing low-frequency oscillation components. These components must be filtered; in this case, the filtered quantities V_1 and V_2 phasors are called "quasi-steady state" phasor voltages.

The Energy Function will be $V_E(t) = V_{KE}(t) + V_{PE}(t)$.

$$V_{PE} = \frac{V_1 V_2}{x'_e}(\cos(\theta_{qss}) - \cos(\theta) + sen(\theta_{qss})x(\theta_{qss} - \theta) \quad (7)$$

$$V_{KE} = H\Omega\omega^2 \quad (8)$$

Where: θ_{qss} is obtained, in practice, by the bandpass filter at measurement angle θ.

VI. METHODOLOGY

Initially, the work carried out electromechanical simulations to verify the presence of CF immediately after simulating short-circuit events in the AC network, considering the operation of the six bipoles in the BIPS. Subsequently, the RBF neural network was used to classify the CF. In the third stage of the work development, the impact of CF on the AC network was verified, and, to this end, the transient instability criterion in the significant Brazilian CNS was analyzed through the stability margin obtained by the Lyapunov FET via simulated PMU data. The electromechanical simulation was performed using the Anatem software from Cepel [11], considering the BIPS monthly scenario power flow cases for the entire year 2020 (12 months) and for the whole of the year 2021 (12 months), with light, medium, and heavy load levels. With this, 36 simulations were obtained for each year, with each simulation corresponding to a CF.

Each simulation's highest value of MIIF, PI, SCR, and MISCR of each busbar interaction was adopted as a selection criterion, as seen in each row of Table I. Table II presents cases where one or two simultaneous CFs occur (CF=1 and CF>=2, respectively), with the value 0 indicating no failure and the value 1 in the appropriate column indicating a commutation failure. Only the highest PI value was presented. Thus, for each month, 12 samples were obtained for each input, with 202 samples (70%) for training the RBF, considering the whole year of 2020 and 86 samples for the operation stage (test), the entire year of 2021. The criterion adopted for the output class was "1" if PI>0.4; otherwise, "0" for PI <=0.4.

The LTEF was computed to evaluate the impact of a CF on the NSC BIPS. The primary purpose was to assess the dynamic behavior of the AC power grid right after the CF. The LTEF was not used to perform RBF training/operation but rather to provide one more safety measure to the operators of the power system control centers in a predictive manner.

Table I – Data obtained via Simulation with Anatem – April 2021

Busbar	MIIF				PI				Pdc[MW]	Scc[MVA]	SCR	MISCR
Heavy Load	IBIUNA-SP345	ARARQ2-SP500	ESTREI-MG500	T.RIO--RJ500	IBIUNA-SP345	ARARQ2-SP500	ESTREI-MG500	T.RIO--RJ500	IBIUNA-SP345	ARARQ2-SP500	ESTREI-MG500	T.RIO--RJ500
IBIUNA-SP345	1.000	0.380	0.265	0.335	1.000	0.725	0.346	0.433	2934.560	21077.820	7.159	2.860
ARARQ2-SP500	0.510	1.000	0.403	0.419	0.268	1.000	0.276	0.284	5588.120	25662.780	4.592	2.512
ESTREI-MG500	0.318	0.354	1.000	0.304	0.244	0.517	1.000	0.301	3826.200	20655.970	5.399	2.618
T.RIO--RJ500	0.287	0.270	0.220	1.000	0.222	0.398	0.222	1.000	3789.790	18099.660	4.776	2.593
Medium Load	IBIUNA-SP345	ARARQ2-SP500	ESTREI-MG500	T.RIO--RJ500	IBIUNA-SP345	ARARQ2-SP500	ESTREI-MG500	T.RIO--RJ500	IBIUNA-SP345	ARARQ2-SP500	ESTREI-MG500	T.RIO--RJ500
IBIUNA-SP345	1.000	0.397	0.275	0.331	1.000	0.650	0.309	0.368	3410.930	20952.150	6.143	2.639
ARARQ2-SP500	0.527	1.000	0.410	0.410	0.322	1.000	0.281	0.278	5588.120	25389.340	4.543	2.416
ESTREI-MG500	0.336	0.369	1.000	0.303	0.299	0.539	1.000	0.300	3826.190	20395.500	5.331	2.493
T.RIO--RJ500	0.301	0.283	0.229	1.000	0.271	0.417	0.231	1.000	3789.780	18212.570	4.806	2.504
Light Load	IBIUNA-SP345	ARARQ2-SP500	ESTREI-MG500	T.RIO--RJ500	IBIUNA-SP345	ARARQ2-SP500	ESTREI-MG500	T.RIO--RJ500	IBIUNA-SP345	ARARQ2-SP500	ESTREI-MG500	T.RIO--RJ500
IBIUNA-SP345	1.000	0.383	0.308	0.313	1.000	0.741	0.527	0.531	1970.920	20326.960	10.314	3.683
ARARQ2-SP500	0.419	1.000	0.424	0.334	0.216	1.000	0.374	0.292	3816.950	22702.640	5.948	3.157
ESTREI-MG500	0.269	0.339	1.000	0.273	0.158	0.385	1.000	0.271	3366.980	18384.230	5.460	3.008
T.RIO--RJ500	0.250	0.243	0.249	1.000	0.148	0.277	0.251	1.000	3339.130	17084.160	5.116	3.051

Table II – Input and Output Data (Class) for RBF – April 2021

Heavy Load	MIIF	PI	SCR	MISCR	Pdc	FC=1	FC>=2
IBIUNA-SP345	0.380	0.725	7.159	2.860	2934.56	0	1
ARARQ2-SP500	0.419	0.284	4.592	2.512	5588.120	0	0
ESTREI-MG500	0.354	0.517	5.399	2.618	3826.200	0	0
T.RIO--RJ500	0.287	0.398	4.776	2.593	3789.790	0	0
Medium Load	**MIIF**	**PI**	**SCR**	**MISCR**	**Pdc**	**FC=1**	**FC>=2**
IBIUNA-SP345	0.397	0.650	6.143	2.639	3410.930	1	0
ARARQ2-SP500	0.527	0.322	4.543	2.416	5588.120	0	0
ESTREI-MG500	0.369	0.539	5.331	2.493	3826.190	1	0
T.RIO--RJ500	0.301	0.417	4.806	2.504	3789.780	1	0
Light Load	**MIIF**	**PI**	**SCR**	**MISCR**	**Pdc**	**FC=1**	**FC>=2**
IBIUNA-SP345	0.383	0.741	10.314	3.683	1970.920	0	1
ARARQ2-SP500	0.419	0.374	5.948	3.157	3816.950	0	0
ESTREI-MG500	0.339	0.385	5.460	3.008	3366.980	0	0
T.RIO--RJ500	0.250	0.277	5.116	3.051	3339.130	0	0

VII. SIMULATIONS AND RESULTS

A. Commutation Failure Simulation using Anatem

For the CF simulation in Anatem software, via the "APFC" internal command, the simulation sequence was adopted to produce multi-infeed CF according to the records of an actual SCF event in BIPS. The faults were applied at AC busbars as indicated by letters (A to E), according to Figure 5, being:
1) Application of three-phase short-circuit at the Ibiuna (A) 525 kV busbar, at time instant t = 200 ms, with a voltage drop of 35%; 2) Application of the CF at Ibiuna at t = 200 ms, with CF duration of t = 72 ms; 3) CF application at Estreito (B) at t = 209 ms, with a CF duration of t = 8 ms; 4) CF application at Madeira's bipole 2 (C) at t = 210 ms, with a CF duration of 48 ms; 5) CF application at the Rio Terminal bipole (D) at t = 211 ms, with a CF duration of 8 ms; 6) Application of CF at Madeira Bipole 1 at t = 211 ms, with a CF duration of 8 ms; 7) CF removal at Estreito at t = 217 ms; 8) CF removal at Rio Terminal at t = 219 ms; 9) CF removal at Madeira Bipole 1 at t = 219 ms 10) removal of CF at Madeira's bipole two at t = 258 ms; 11) removal of CF at Ibiuna at t = 272 ms; 12) opening of LT 525 kV Ibiuna – Bateias C1 and C2 (E) and 13) remove the short-circuit at t = 300 ms.

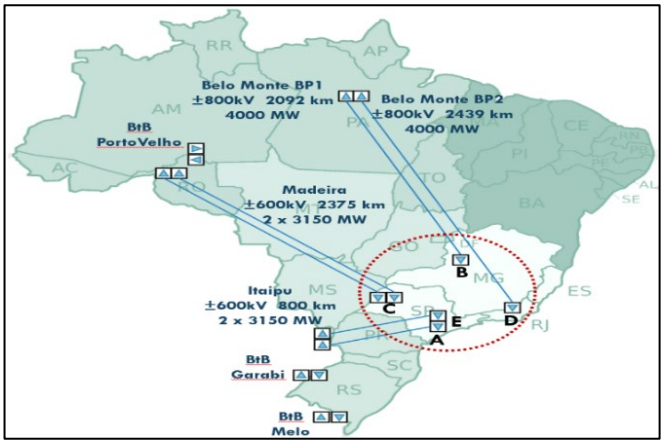

Fig. 5 – Bipoles AC Busbars

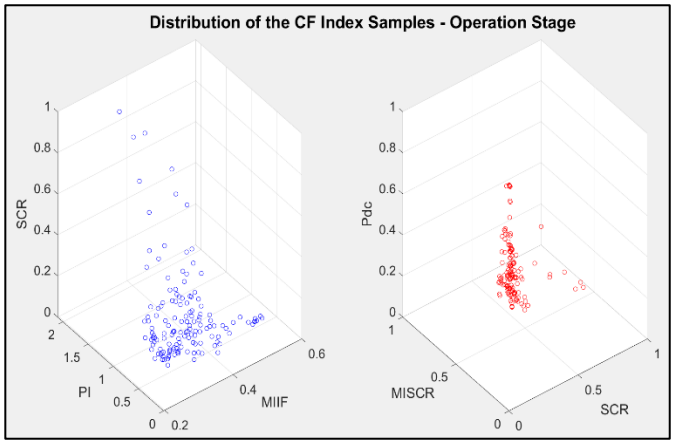

Fig. 7 - RBF input samples: MIIF, PI, SCR, MISCR, and Pdc – Operation Stage

B. Distribution of the Sampes from Training and Operation Stages of the RBF

Figures 6 and 7 show the distribution of samples used in the RBF network. For the training stage, 202 samples were used - available between January and December 2020, and for the operation stage, 86 samples were used - between January and December 2021.

The samples used were MIIF, PI, SCR, MISCR, and Pdc. An ANN's processing is parallel, but the knowledge is distributed, so one should eliminate the so-called outliers, guaranteeing the robustness of the network to be trained.

Several techniques are used for this purpose, such as statistical distribution and loss of monotonicity, and, in some cases, external agents are used to eliminate these outliers. In this work, the data quality analysis filter of the Weka tool [18], *InfoGain*, was used. This filter removes redundant attributes, determines a subset of the most relevant characteristics for representing the problem, and improves the performance of the RBF.

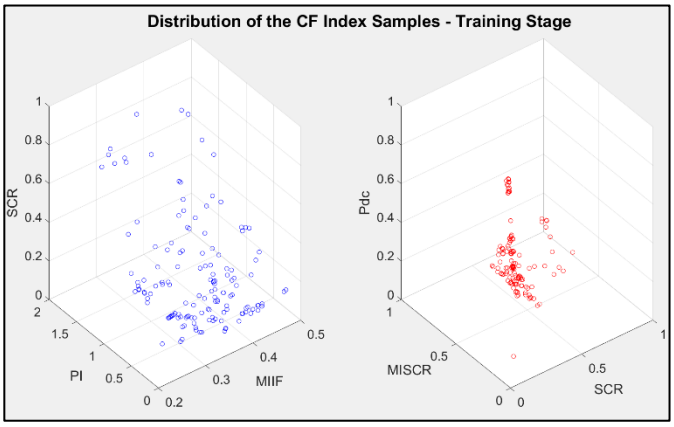

Fig. 6 - RBF input samples: MIIF, PI, SCR, MISCR, and Pdc – Training Stage

C. RBF Network Implementation Results

The RBF network was developed and implemented in a Matlab environment without a toolbox. Five data inputs were used: MIIF, PI, SCR, MISCR, and Pdc. A total of 10 neurons were used for the intermediate layer (10 clusters). The network's processing time in the training step was t = 613 ms. The clusters of the intermediate neural layer and the variances are presented in Table III. The synaptic weights of the second neural layer were: [-0.3835, 0.722, 0.9275, 0.2016, 0.522, 0.6778, 0.8173, -1.8606, 0.8331, -0.6577, 0.8499].

Table III – Centroids and Variances

Centroids W_1					Variances
0.4106	0.8847	0.2274	0.2309	0.3451	0.2012
0.4172	0.3056	0.0772	0.1159	0.9924	0.0277
0.3568	0.6210	0.1483	0.1612	0.5029	0.1254
0.2704	0.5860	0.4020	0.4766	0.1968	0.2020
0.3638	0.5288	0.1135	0.1420	0.6560	0.1005
0.4505	0.2588	0.0845	0.1257	0.9339	0.0355
0.4454	1.5091	0.4043	0.2690	0.2383	0.3287
0.3229	0.2161	0.1762	0.2971	0.4689	0.1744
0.2678	0.9768	0.8887	0.8318	0.0881	0.3181
0.3798	0.1917	0.0749	0.1230	0.9818	0.0338

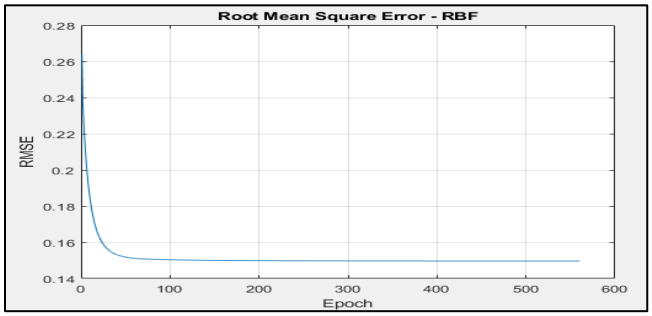

Fig. 8 – Root Mean Square Error

Figure 8 shows the Root Mean Square Error (RMSE) for the operation step with CF=1, with 582 epochs after the neural network's convergence. The hit rate in the operation step was 90% for the condition CF=1 and 91% for the condition CF>=2.

D. Lyapunov Transient Energy Function

With the inertia data per geoelectric area, in MW.s dimensional unit, obtained through the state estimator in the BIPS, it was possible to find the equivalent inertia between the regions, in MW.s p.u., in the 100 MVA base. Only the NSC was considered to obtain the results. Figure 9 shows the NSC Inertia Equivalent from 2020 to 2021, and Figure 10 shows the period of 2021 – 2022.

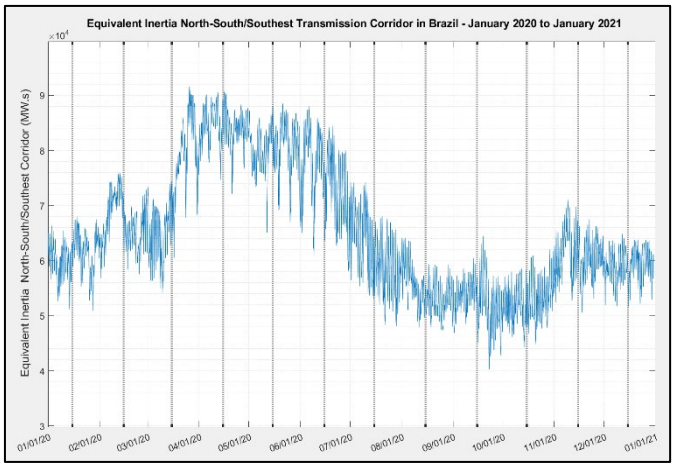

Fig. 9 – Equivalent Inertia NSC (2020 – 2021)

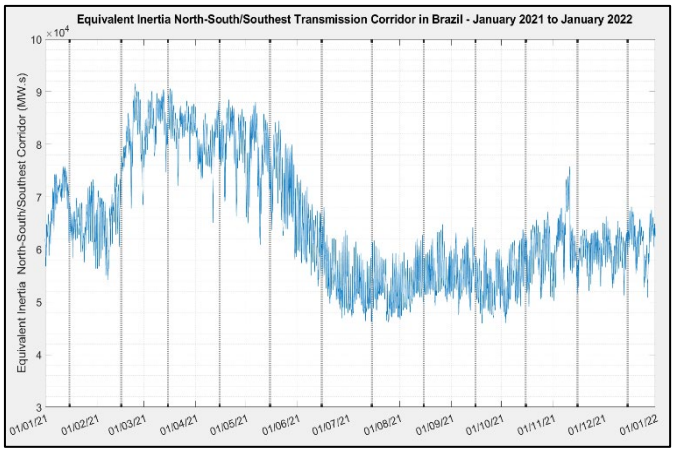

Fig. 10 – Equivalent Inertia NSC (2021 – 2022)

E. Angular and Frequency Differença in the NSC

Figures 11 and 12 show the differences in the NSC's frequency and angle for the medium load scenario 2021.

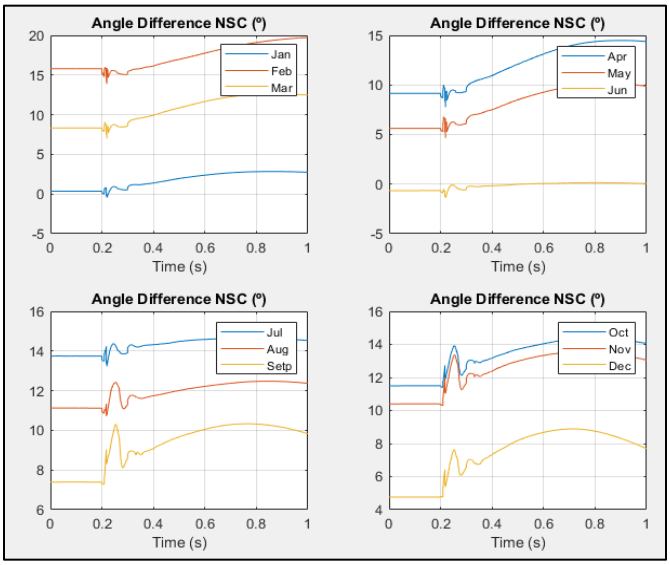

Fig. 11 – Medium Load Scenario – 2021. Angle Difference at NSC

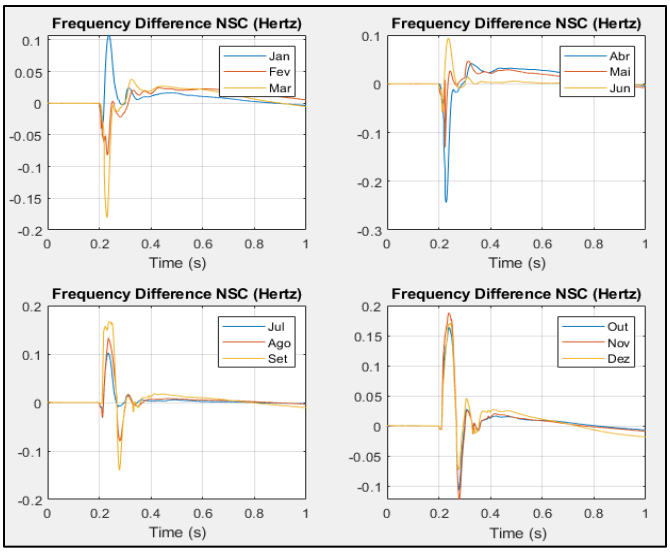

Fig. 12 – Medium Load Scenario – 2021. Frequency Difference at NSC

Observing the variations of the values when the CF starts, and the maximum values are reached is possible. Due to the large number of scenarios analyzed, only the LTEF for the year 2021 will be shown in the Figures below.

F. Lyapunov Transient Energy Function Results

According to [11], a transient instability condition can be computed as: $V_{PE}(\delta^u) - V_{PE}(\delta^{cl}) > V_{KE}^{cl}$ [9], where $V_{PE}(\delta^u)$represents the PE of an unstable operation point, $V_{PE}(\delta^{cl})$ and V_{KE}^{cl} the PE and KE at the instant of fault elimination.

Figures 13, 14, and 15 show the LTEF considering the heavy and medium load of 2021. Table IV shows the LTEF and its severity in the NSC right after the CF, indicating possible transient instability conditions. The critical value adopted for PE in the NSC was $V_{PE}(\delta^u) = 2.5\ pu - MW - rad/s$. This value was obtained considering the disturbance analysis of a real case in the BIPS, particularly one disturbance on March 03, 2018, in BIPS with a massive blackout involving the transient instability in the CNS, and it was obtained through electromechanical simulation considering the load flow of the pre-fault blackout event. According to Table IV, for April 2021 with the heavy load scenario, there is an indication of the occurrence of transient instability in the NSC right after a SCF, which can be corroborated with the result presented in Table II, where when an electrical fault occurs at the Ibiúna busbar (345 kV), located near the Itaipu HVDC, there is the possibility of a SCF. It is essential to consider that SCF can occur in the BIPS; however, the impact on the AC network may not be as significant. Therefore, this work identifies commutation failures in BIPS, with various load and generation scenarios, but also shows the impacts on the AC network. For example, as a mitigation action for this April month case, it could dispatch power through the HVDC links, bringing the interaction potential index to values lower than 0.4. Since, even today, control mitigation actions are not sufficient to prevent a CF in the thyristor valves, mainly because the times involved are speedy (order of a few milliseconds), a predictive action such as power dispatch by HVDC-LCC connections is a viable solution. Thus, using a suitable trained neural network during the network's operation phase, whose inputs can be measured values, it is possible to verify the need for such a power dispatch to avoid a CF, especially in cases where such a CF can lead an important transmission corridor to operate in an unstable operating condition.

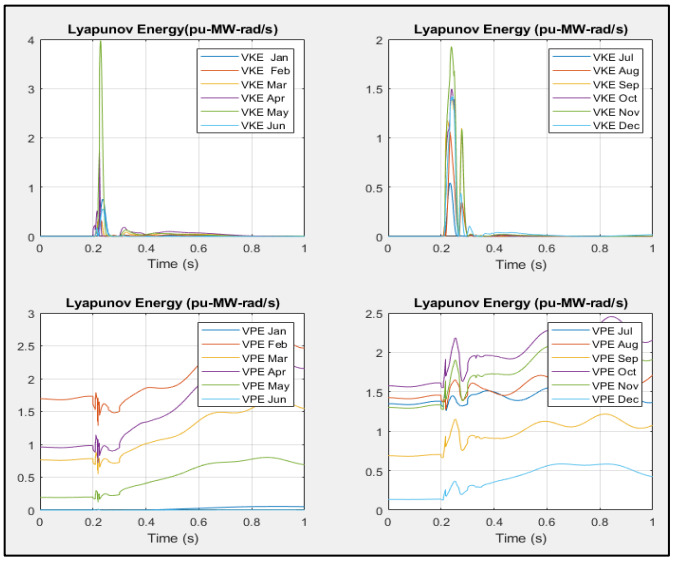

Fig.13 – LTEF – Heavy Load Scenario 2021

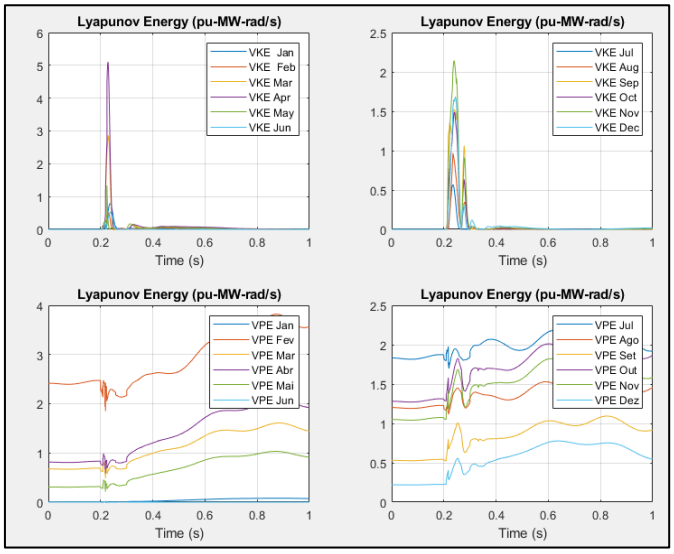

Fig. 14 – LTEF – Medium Load Scenario 2021

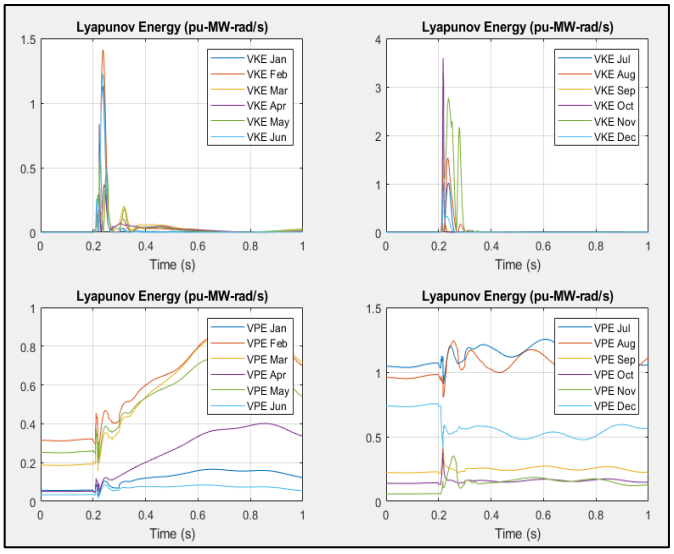

Fig.15 – LTEF – Light Load Scenario 2021

Table IV – Severity – NSC Operation After CF

Year	VKE (pu-MW rad/s)			VPE (pu-MW rad/s)			Severity		
2021	Heavy	Medium	Light	Heavy	Medium	Light	Heavy	Medium	Light
Jan	0.79	0.75	1.12	0.1	0.02	0.03	0	0	0
Feb	0.45	0.3	1.41	1.85	1.28	0.47	0	0	0
Mar	2.86	0.3	0.38	0.59	0.55	0.36	1	0	0
Apr	5.1	1.78	0.75	0.71	0.78	0.04	1	0	0
May	1.34	3.86	0.6	0.43	0.3	0.37	0	1	0
Jun	0.53	0.56	1.22	0.1	0.02	0.35	0	0	0
Jul	0.57	0.54	1	1.74	1.45	1.21	0	0	0
Aug	0.97	1.1	1.53	1.45	1.65	1.24	0	0	0
Sep	1.52	1.4	2.19	1	1.15	0.39	0	0	0
Oct	1.5	1.5	3.6	1.82	2.18	0.38	1	1	1
Nov	2.14	1.93	2.77	1.68	1.9	0.35	1	1	1
Dec	1.68	1.4	0.85	0.55	0.36	0.41	0	0	0

VIII. Conclusions

This work presented a new proposal for using artificial neural networks to mitigate commutation failures in HVDC-LCC links in the multi-infeed scenario in the BIPS. As a complementary analysis, LTEF was used for the post-event analysis in the NSC in Brazil. The RBF ANN proved robust and had a significant hit rate for single and multiple CF cases, which is adequate for this pattern recognition application. The criterion adopted for training the RBF ANN considered the commutation failure rates made available by CEPEL's Anatem tool, and the network data were in a compact convex region (closed and bounded) after the clustering performed in the first training stage. Since it is possible to obtain the power flow and perform the electromechanical simulation in a real-time scenario, it is then possible to get the CF indexes in real time, feeding back the inputs of the already trained RBF ANN for the operation stage.

Since the equivalent inertia between geoelectric regions in the BIPS is also monitored online, monitoring the frequency and angle differences in the BIPS's main transmission corridors would be enough to calculate the LTEF's stability margins in real time.

Synchrophasor data can easily be obtained from the busbars and circuits of the transmission lines of the main transmission corridors of the BIPS. However, using such data in this work was not possible because they belong to the TSO owners. In any case, Anatem provided the data in phasor format, and the software adjusted the frame rate to 1 per cycle.

Thus, with the promising results obtained from this work, there is the possibility of providing subsidies for predictive analyses to control center operators for real-time decision-making when facing the CF problem.

Acknowledgment

This study was supported by the research agencies CNPq (307237-2020/6), FAPESP (2022/01896-7) and CAPES (code 001). The authors are with the School of Electrical and Computer Engineering at the University of Campinas, Brazil.

References

[1] S.R.Lígia, “Automatic Computing of Multi-Infeed Predictive Indexes Providing Situational Awareness in Real-Time Operation of Hybrid AC-HVDC Systems," Cigre e-Session August 28, 2020.

[2] I. Oketch, "Commutation Failure Prevention for HVDC," the Chalmers University of Technology Gothenburg, Sweden 2016.

[3] S. Mirsaeidi, X. Dong, D. Tzelepis, D. M. Said, A. Dyśko and C. Booth, "A Predictive Control Strategy for Mitigation of Commutation Failure in LCC-Based HVDC Systems," in IEEE Transactions on Power Electronics, vol. 34, no. 1, pp. 160-172, Jan. 2019, doi: 10.1109/TPEL.2018.2820152.

[4] T. Machida and Y. Yoshida, "A method to detect the deionization margin angle and to prevent the commutation failure of an inverter for DC transmission," IEEE Trans. Power App. Syst., vol. PAS-86, no. 3, pp. 259-262, Mar. 1967.

[5] S. Tamai, H. Naitoh, F. Ishiguro, M. Sato, K. Yamaji and N. Honjo, "Fast and predictive HVDC extinction angle control," IEEE Trans. Power Syst., vol. 12, no. 3, pp. 1268-1275, Aug. 1997.

[6] A. Hansen and H. Havemann, "Decreasing the commutation failure frequency in HVDC transmission systems," IEEE Trans. Power Del., vol. 15, no. 3, pp. 1022-1026, Jul. 2000.

[7] L. Zhang and L. Dofnas, "A novel method to mitigate commutation failures in HVDC systems," Proc. Int. Conf. Power Syst. Technol., vol. 1, pp. 51-56, 2002.

[8] CIGRE Working Group B4.41. Systems with Multiple DC Infeed. Available at: https://e-cigre.org/publication/364-systems-with-multiple-dc-infeed (accessed on 13/12/2021).

[9] Synchrophasor Measurements for Power Systems, IEEE Standard C37.118.1, Dec. 2011.

[10] Synchrophasor Measurements for Power Systems – Amendment 1: Modification of Selected Performance Requirements, IEEE Standard C37.118a, Apr. 2014.

[11] Anatem - Electromechanical Transient Analysis, CEPEL. Available at: https://see.cepel.br/manual/anatem/index.html, accessed on January 15, 2024.

[12] I.N.da Silva, D.H. Spatti, R.A. Flauzino, L.H.B.Liboni, S.F.R.Alves, “Artificial Neural Networks: A Practical Course” 1st ed. 2017.

[13] M. A. Pai, "Energy Function Analysis of Power System Stability," ed, 1989.

[14] M. Pavella, D. Ernst, and D. Ruiz-Vega, "Transient Stability of Power Systems. A unified Approach to Assessment and Control, Kluwer's Power Electronics and Power System Series," SECS581 0-7923-7963-2, 2000.

[15] J. H. Chow, A. Chakrabortty, M. Arcak, B. Bhargava, and A. Salazar, "Synchronized phasor data-based energy function analysis of dominant power transfer paths in large power systems," IEEE Transactions on Power Systems, vol. 22, no. 2, pp. 727-734, 2007.

[16] I. Dobson, "New angles for monitoring areas," in Bulk Power System Dynamics and Control (iREP)-VIII (iREP), 2010 iREP Symposium, 2010: IEEE, pp. 1-13.

[17] I. Dobson et al., "Electric power transfer capability: concepts, applications, sensitivity and uncertainty," PSERC Publication, 01-34, 2001.

[18] Weka Tool “Waikato Environment for Knowledge Analysis”. Available at: https://www.cs.waikato.ac.nz/ml/weka/ (accessed on January 15, 2024).